AIAA 80-1879R

Analysis of Thrust-Induced Effects on the Longitudinal Aerodynamics of STOL Fighter Configurations

J.W. Paulson Jr.*
NASA Langley Research Center, Hampton, Va.

An analysis of the thrust-induced longitudinal aerodynamic characteristics of three fighter-type configurations is presented. A brief discussion of the takeoff and landing requirements for the next generation of fighter aircraft leads to the conclusion that advances in lift coefficient and thrust reversing will be required to allow short-field operation. Typical power-on longitudinal aerodynamic data for the three fighter configurations, indicating different approaches to meeting the high-lift coefficient requirement, are discussed. Thrust reversing is not addressed in this paper. The power-on data are analyzed to determine what power effects are present, that is, direct thrust, boundary-layer control, vortex flows, or induced circulation. The results of the analysis indicate, for the configurations studied, that induced effects are small compared to direct thrust. Also, the thrust induced effects may be boundary-layer control, leading-edge vortex flows or induced circulation, depending on the configuration.

Nomenclature

a = acceleration, m/s^2 (ft/s^2)
$\bar{c}$ = mean aerodynamic chord, m (ft)
C_D = drag coefficient = (force in drag direction)/qS
C_L = lift coefficient = (force in lift direction)/qS
C_m = pitching-moment coefficient = (pitching moment)/$qS\bar{c}$
C_T = thrust coefficient = (static thrust)/qS
g = gravitational constant = 9.807 m/s^2 (32.174 ft/s^2)
T/W = thrust-to-weight ratio
W/S = wing loading, kN/m^2 (lbf/ft^2)
$\bar{x}$ = distance between moment reference center and longitudinal location of the center of the resultant thrust vector, m (ft)
α = angle of attack, deg
Λ = sweep angle, deg
δ = deflection angle, deg
$\Delta C_{D,\Gamma}$ = increment in drag coefficient due to thrust-induced effects = $C_D + C_T \cos(\alpha+\delta_N) - C_D|_{C_T=0}$
$\Delta C_{L,\Gamma}$ = increment in lift coefficient due to thrust-induced effects = $C_L - C_T \sin(\alpha+\delta_N) - C_L|_{C_T=0}$
$\Delta C_{m,\Gamma}$ = increment in pitching-moment coefficient due to thrust-induced effects = $C_m + x/c\, C_T \sin_N - C_m|_{C_T=0}$

Subscripts

f = flaps
N = nozzles
SWB = spanwise blowing

Introduction

RECENTLY, interest in STOL performance for combat aircraft has been renewed; not only for Navy V/STOL aircraft, but also for future Air Force combat aircraft. The Air Force interest arises from the possible need to operate aircraft from damaged airfields in Western Europe where bomb craters may reduce available runway lengths. Thus the Air Force STOL requirement may be one of operating aircraft out of 305-m (1000-ft) or shorter sections of damaged runways. While some of today's fighter aircraft can make this takeoff distance when lightly loaded, none can approach this sort of landing length under normal weight conditions (Fig. 1). It appears that large improvements in both aerodynamics and thrust reversing will be required to allow operation from this short runway length for any but the lightest aircraft loading (Fig. 2).

There are several approaches which utilize thrust effects to improve the aerodynamics of fighter configurations. Vectoring the engine exhaust or bleeding engine air for spanwise blowing or flap boundary-layer control (BLC) are promising methods. These methods show improvements in aerodynamics through direct engine thrust effects, BLC, vortex flows, and induced circulation effects.

Three configurations have been studied in the NASA Langley 4- by 7-Meter Tunnel to assess the STOL performance of fighter aircraft. One configuration shown in Fig. 3 was an in-house wing-canard research model having a wing sweep of 50 deg and aspect ratio of 3.26. Power was provided through two-dimensional vectoring nozzles at the wing root. Aerodynamic and performance results have been published.[1-3] The second concept (Fig. 4) was tested in a cooperative program conducted by NASA, the U.S. Air Force Wright Aeronautical Laboratory, and General Dynamics. The configuration was a vectored-engine-over-wing (VEO-wing) concept with a wing sweep of 40 deg and an aspect ratio of 3.5. This configuration, which employed spanwise blowing in combination with the main two-dimensional vectoring nozzles, has been reported in several references.[4-8] The third concept was tested in a cooperative program conducted by NASA, the U.S. Air Force Wright Aeronautical Laboratory, and the Boeing Aircraft Co. The concept is shown in Fig. 5 and is a supersonic cruise concept with a wing sweep of 68 deg and an aspect ratio of 1.5. Power was provided through two-dimensional vectoring nozzles under the wing trailing edge in combination with a nose jet for trim. The power-on aerodynamics for each configuration, shown in Figs. 6-8, indicates improvements in lift curve, maximum lift coefficient, and lift-drag polars typical of vectored-thrust configurations. This paper will attempt to assess whether these improvements are due to direct thrust effects, BLC, leading-edge vortex flows, or induced circulation.

Presented as Paper 80-1879 at the AIAA Aircraft Systems and Technology Meeting, Anaheim, Calif., Aug. 4-6, 1980; submitted Sept. 9, 1980; revision received April 22, 1981.

*Aero-Space Technologist, Low-Speed Aerodynamics Branch, Subsonic-Transonic Aerodynamics Division. Member AIAA.

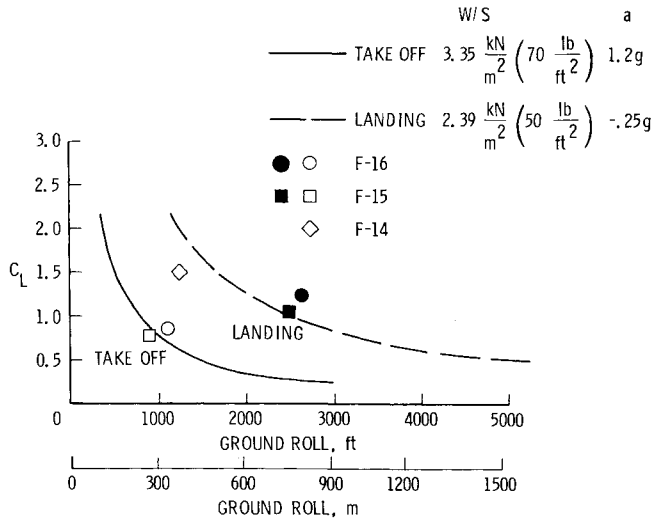

Fig. 1 Takeoff and landing ground rolls for typical fighter aircraft.

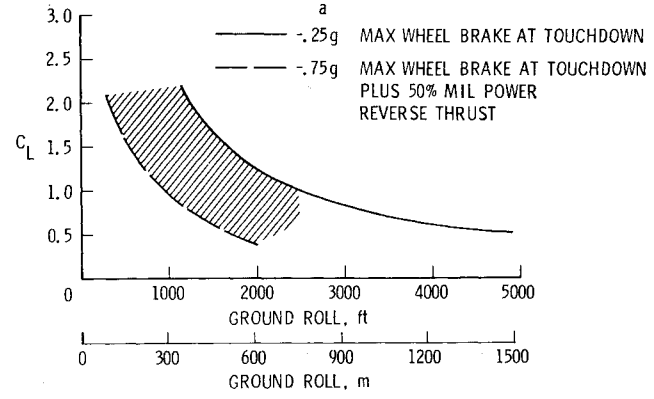

Fig. 2 Effect of lift coefficient and thrust reverser on landing ground roll.

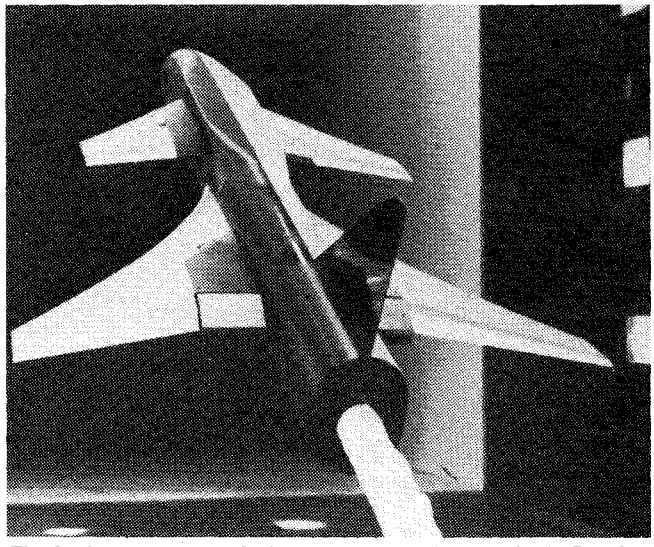

Fig. 3 In-house powered wing-canard model installed in the Langley 4- by 7-Meter Tunnel.

Discussion

Thrust Removed Aerodynamic Coefficients

In order to assess the thrust-induced effects, the direct thrust component of the aerodynamics, as well as the power-off configuration aerodynamics, must be removed as follows:

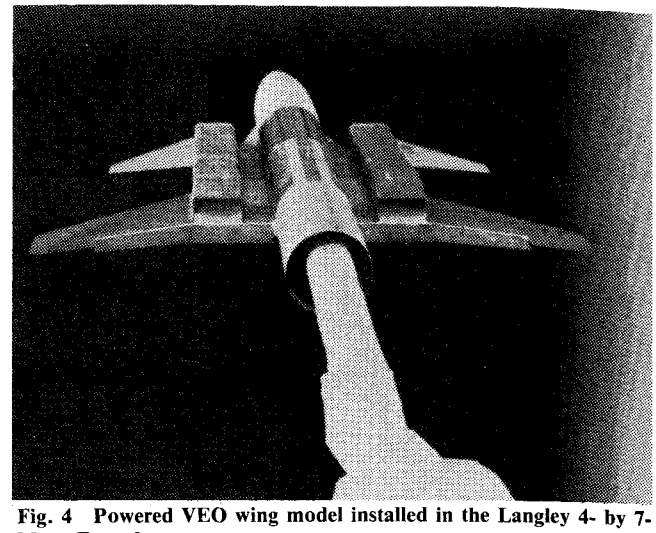

Fig. 4 Powered VEO wing model installed in the Langley 4- by 7-Meter Tunnel.

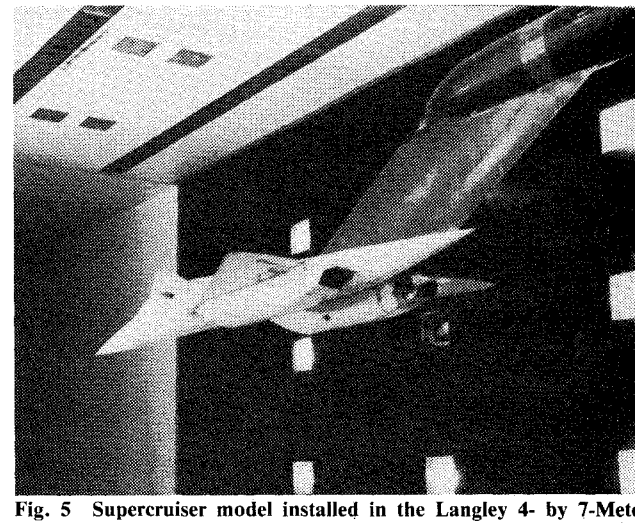

Fig. 5 Supercruiser model installed in the Langley 4- by 7-Meter Tunnel.

$$\Delta C_{L,\Gamma} = C_L|_{C_{T\geq 0}} - C_T \sin(\alpha+\delta_j) - C_L|_{C_{T=0}}$$

$$\Delta C_{D,\Gamma} = C_D|_{C_{T\geq 0}} - C_T \sin(\alpha+\delta_j) - C_D|_{C_{T=0}}$$

$$\Delta C_{m,\Gamma} = C_m|_{C_{T\geq 0}} + \bar{x}/\bar{c}\ C_T \sin\delta_j - C_m|_{C_{T=0}}$$

where C_L, C_D, and C_m are measured aerodynamic coefficients at the resultant power-off and power-on conditions, δ_j is the resultant thrust vector angle, C_T is the thrust coefficient, and $\bar{x}/\bar{c}$ is the distance from the resultant thrust vector to the model moment reference center. Therefore $\Delta C_{L,\Gamma}$, $\Delta C_{D,\Gamma}$, and $\Delta C_{m,\Gamma}$ are the increment of lift, drag, and pitching-moment coefficients due to thrust-induced effects.

In-House Fighter Configuration

Induced aerodynamic coefficients are presented in Fig. 9 for the in-house wing-canard fighter configuration. These induced coefficients are plotted against C_T in order to determine whether BLC and/or induced circulation were present on this configuration. It is seen in the figure that the $\Delta C_{L,\Gamma}$ data have a high slope region for C_T below 0.2, indicating that the primary induced effect is boundary-layer control attaching the flow on the nozzles and inboard portions of the trailing-edge flap. Above $C_T = 0.2$, the data tend to be constant indicating that no further induced effects are present, that is, once the flow is attached on the nozzle and

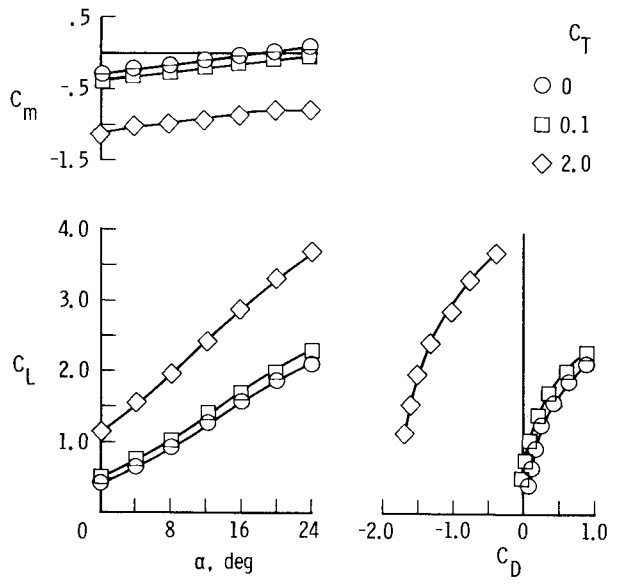

Fig. 6 Powered longitudinal aerodynamics for in-house wing-canard fighter model, $\delta_f = \delta_N = 20$ deg.

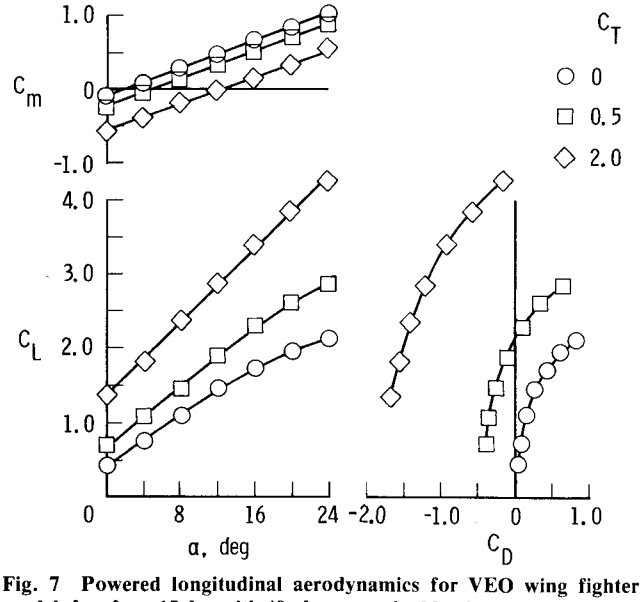

Fig. 7 Powered longitudinal aerodynamics for VEO wing fighter model, $\delta_f = \delta_N = 15$ deg with 40- deg spanwise blowing.

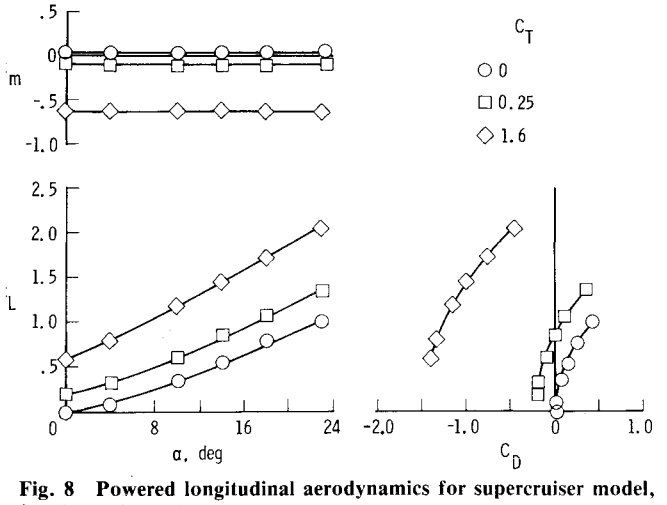

Fig. 8 Powered longitudinal aerodynamics for supercruiser model, $\delta_f = 0$ deg, $\delta_N = 30$ deg.

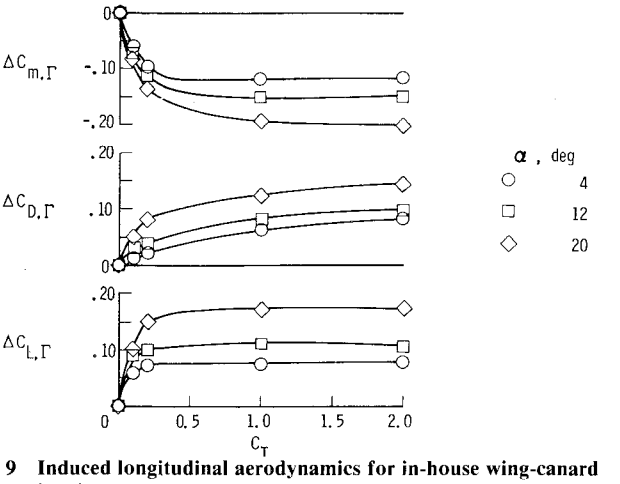

Fig. 9 Induced longitudinal aerodynamics for in-house wing-canard fighter, $\delta_f = \delta_N = 20$ deg at constant angle of attack.

flap, increases in C_T do not produce induced circulation. The increase in $\Delta C_{L,\Gamma}$ as angle of attack is increased, is to be expected as the wing has increasing areas of flow separation which may be reattached by the nozzle flow. A verification of this trend is found in the induced pitching-moment coefficients. If the thrust-induced effects are confined to the area near the nozzle/flap then a unit of $\Delta C_{L,\Gamma}$ should produce about $\Delta C_{m,\Gamma} \simeq -1.07\ \Delta C_{L,\Gamma}$. This follows by noting that the distance from the moment reference center to the nozzle/flap hinge line is approximately 1.07 $\bar{c}$. In fact, most of the data show $\Delta C_{m,\Gamma}$ equal to from -1.1 to -1.2 times $\Delta C_{L,\Gamma}$, indicating that lift is being generated aft of the nozzle/flap hinge line rather than forward on the wing as would be the case if induced circulation effects were present. The increases in drag coefficient are due to increased induced drag as the lift coefficients are increased and some scrubbing drag due to the jet wiping the model fuselage. Therefore, both from the shape of the $\Delta C_{L,\Gamma}$ vs C_T curve and the amount of $\Delta C_{m,\Gamma}$ produced for a given $\Delta C_{L,\Gamma}$, it would appear that the thrust-induced effects on this configuration are confined to the direct thrust component and BLC near the nozzle and inboard flap rather than induced circulation effects. Since there was no spanwise blowing on this configuration, there were no vortex flows expected or indicated in the data.

Vectored Engine Over Wing

Whereas the previous configuration analysis was fairly straightforward, the VEO wing with main nozzles and spanwise blowing nozzles is somewhat more involved owing to the multiple interacting flowfields. The configuration analysis was broken into three separate parts: 1) the main nozzles alone, 2) the spanwise nozzles alone, and 3) the combination of main and spanwise nozzles. Data for each are presented in Figs. 10-15, and the following discussion will begin with the main nozzles alone.

Main Nozzles Alone

Figures 10 and 11 present the induced coefficients for a nozzle and flap deflection of 15 and 30 deg, respectively. As in Fig. 10, the $\Delta C_{L,\Gamma}$ vs C_T data show the high slope region below $C_T \simeq 1.0$ and constant values of $\Delta C_{L,\Gamma}$ above $C_T = 1.0$. This is indicative of a constant induced effect once the flow is established. The magnitude of the $\Delta C_{L,\Gamma}$ in Fig. 9 is slightly higher than that of Fig. 10 owing to configuration effects (i.e., large VEO nacelle with nozzle located on the upper surface forward of the flap hinge line as opposed to the first model with a nozzle at the trailing edge of the flap). The VEO wing nozzle somewhat more effectively generated induced flow on a larger area of the wing. These effects again are a function of the larger region of flow separation at higher angles of attack. As before, the $\Delta C_{D,\Gamma}$ is approximately equal

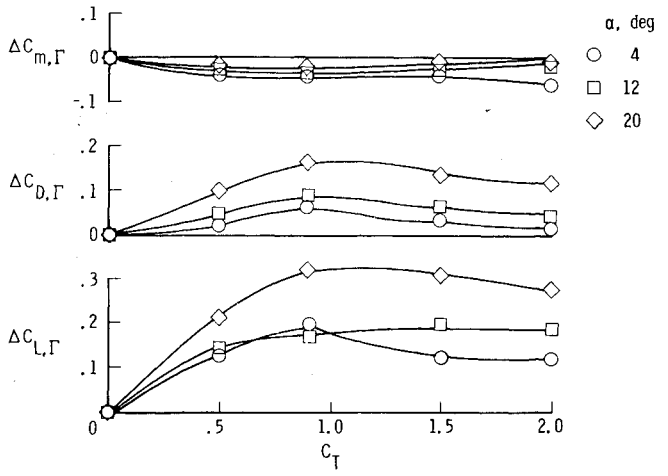

Fig. 10 Induced longitudinal aerodynamics for VEO wing model, $\delta_f = \delta_N = 15$ deg, at constant angle of attack.

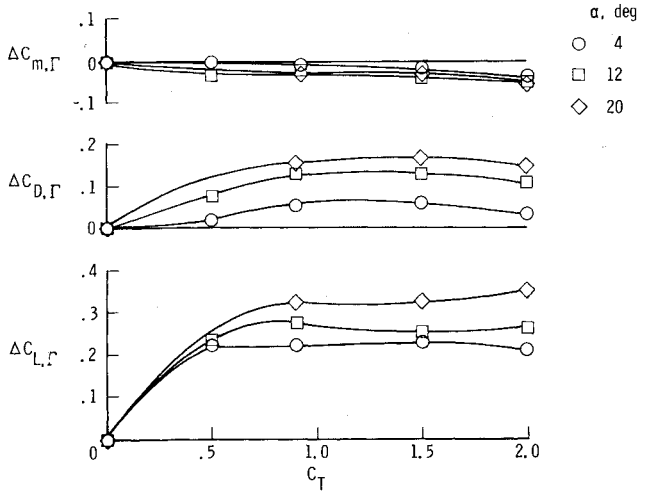

Fig. 11 Induced longitudinal aerodynamics for VEO wing model, $\delta_f = \delta_N = 30$ deg, at constant angle of attack.

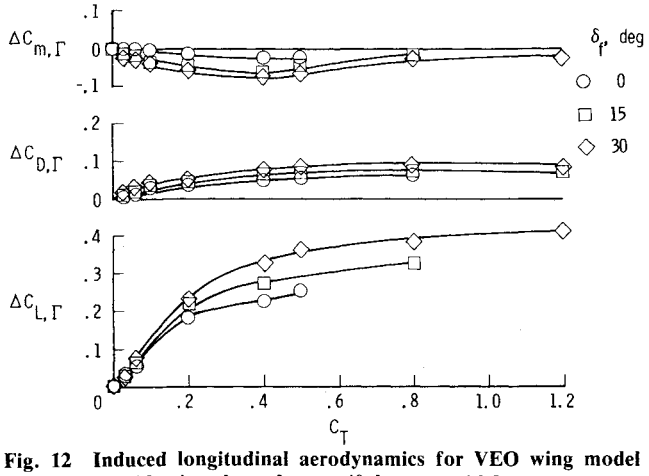

Fig. 12 Induced longitudinal aerodynamics for VEO wing model with spanwise blowing alone, $\delta_{SWB} = 40$ deg at $\alpha = 16$ deg.

to the induced drag that would be expected when the lift coefficient is increased.

As in the previous discussion, it would appear that direct thrust is dominant and that the induced effect is a combination of BLC and induced circulation.

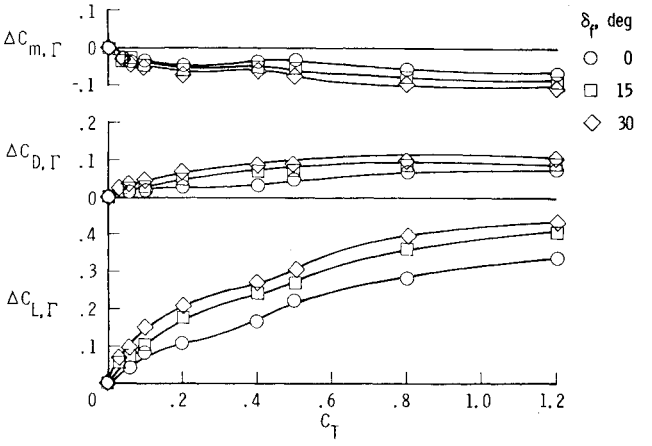

Fig. 13 Induced longitudinal aerodynamics for VEO wing model with spanwise blowing alone, $\delta_{SWB} = 60$ deg at $\alpha = 16$ deg.

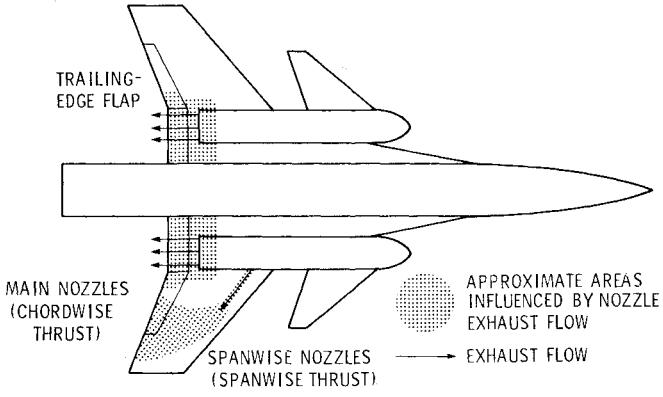

Fig. 14 Sketch of VEO wing configuration showing approximate areas of wing effected by nozzle exhaust flow.

Spanwise Blowing Nozzles Alone

Figures 12 and 13 present induced coefficients for the VEO wing configuration with spanwise blowing nozzles alone at angles of 40 and 60 deg, respectively (i.e., parallel to, and 20 deg aft of wing leading edge). The trends in these data are not as well defined as for the main nozzles because the spanwise jet must mix with the freestream air and the area of the wing affected changes with C_T as the higher energy jet penetrates further along the wing span. In general, however, the $\Delta C_{L,\Gamma}$ show a higher slope region at low C_T and a flattening of the curve as C_T approaches 1.0. These overall effects are a function of flap deflection. This observation supports the idea that at moderate angles of attack the spanwise jet mixes with the free stream and turns over the outboard trailing-edge flap (Fig. 14), thereby increasing flap effectiveness rather than increasing leading-edge vortex flows. These trends are more evident at $\delta_{SWB} = 60$ deg, where the jet is initially directed downstream and loses less energy upon mixing with the free stream, therefore having a greater effect on maintaining attached flow on the flap.

Combined Main Nozzle and Spanwise Blowing Nozzles

Figures 15 and 16 present induced coefficients for the VEO wing configuration with both main and spanwise nozzles. These data are slightly larger than those obtained from the superposition of main nozzles alone and the spanwise blowing nozzles alone. The data, which are a function of angle of attack, show the same trends as before: initial high slope regions which flatten out as C_T is increased above 1.0 and drag levels equal to induced drag due to increased lift coefficients. However, the complex flowfield, limited pressure data, and lack of flow visualization make definitive analysis difficult.

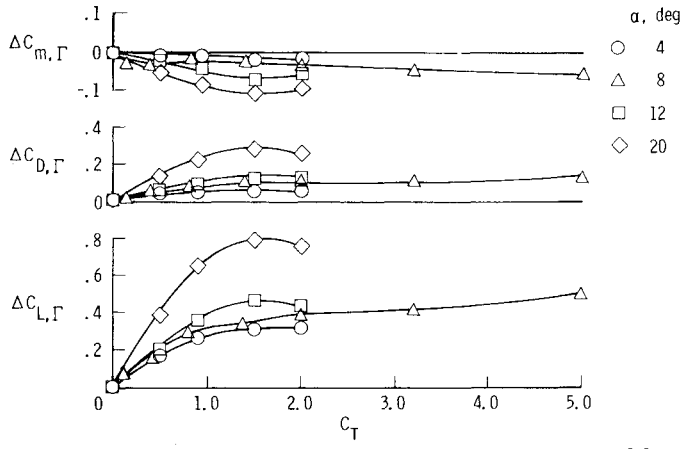

Fig. 15 Induced longitudinal aerodynamics for VEO wing model with chordwise and spanwise blowing, $\delta_f = \delta_N = 15$ deg, $\delta_{SWB} = 40$ deg, at constant angles of attack.

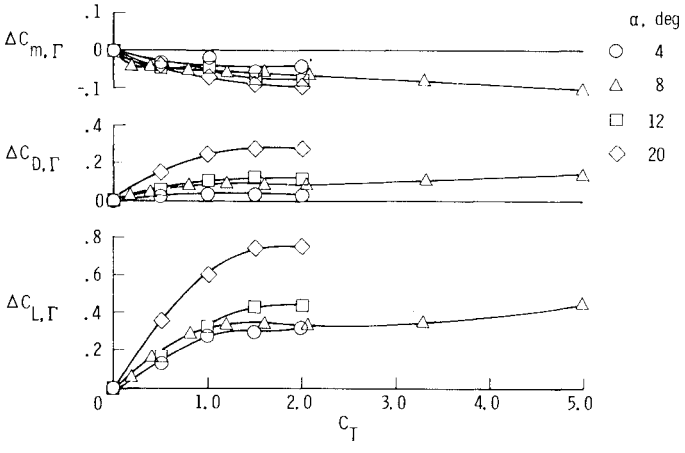

Fig. 16 Induced longitudinal aerodynamics for VEO wing model with chordwise and spanwise blowing, $\delta_f = \delta_N = 15$ deg, $\delta_{SWB} = 60$ deg, at constant angles of attack.

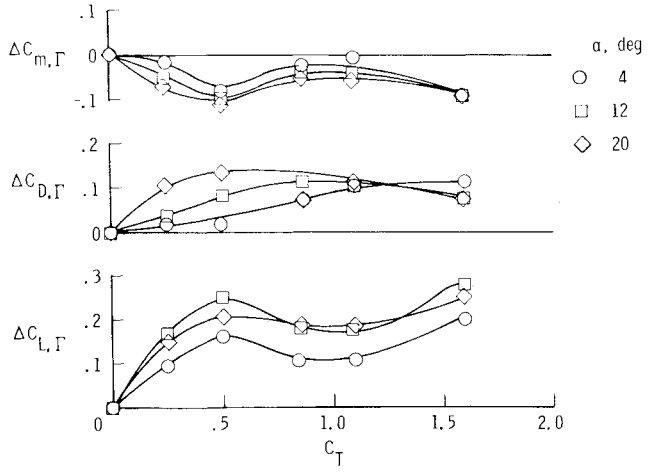

Fig. 17 Induced longitudinal aerodynamics for supercruiser model, $\delta_f = 0$ deg, $\delta_N = 30$ deg, at constant angles of attack.

It would appear that the VEO wing configuration aerodynamics are dominated by direct thrust. The main nozzles and spanwise blowing nozzles tend to help maintain attached flow along the trailing-edge flap system as well as produce induced circulation. Leading-edge vortex flows do not appear to be present at moderate angles of attack.

Supercruiser Configuration

Figure 17 presents the induced coefficients for the supercruiser configuration with an aspect ratio 4 ramp nozzle. These data, which are a function of angle of attack, are somewhat scattered, but again, the same trend is present—initial high slope regions which flatten as C_T increases above 0.5. Nose-down $\Delta C_{m,\Gamma}$ and $\Delta C_{m,\Gamma}/\Delta C_{L,\Gamma} \simeq 0.3$-0.5 indicate aft loading rather than leading-edge loading. Drag levels approximately equal to induced drag due to increased lift coefficients are present, leading to the conclusion that direct thrust predominates with BLC around the nozzle/flap region being the major thrust-induced effect.

Concluding Remarks

Three different fighter configurations have been investigated in the NASA Langley 4- by 7-Meter Tunnel to determine the STOL performance of fighter aircraft. Each was analyzed to determine the effects of power on the induced longitudinal aerodynamics of the configuration. The configurations ranged from moderate wing sweep ($\Lambda = 40$ deg) to high wing sweep ($\Lambda = 68$ deg), from modest aspect ratios (3.5) to very low aspect ratios (1.5), and from over-wing to underwing nozzle placement. Even with this range of configurations, the general trends in the induced effects were consistent. Some specific comments on these effects follow.

1) Induced effects on all three configurations are small as compared to the direct thrust effects.

2) The induced effects on the NASA in-house configuration are primarily associated with the induced effects on BLC around the nozzle and trailing-edge flap system rather than induced circulation.

3) The induced effect on the VEO wing configuration are also associated with BLC around the nozzle and flap system as well as some induced circulation depending on the configuration.

4) The induced effects at moderate angles of attack for the VEO wing configuration with spanwise blowing appear to be associated with the spanwise jet turning downstream and flowing over the trailing-edge flap system rather than intensifying leading-edge vortex flows.

5) The induced effects for the supercruiser configuration are primarily associated with BLC around the nozzle and trailing-edge flap system.

References

[1] Paulson, J.W. Jr. and Thomas, J.T., "Summary of Low-Speed Longitudinal Aerodynamics of Two Powered Close-Coupled Wing-Canard Fighter Configurations," NASA TP 1535, Dec. 1979.

[2] Paulson, J.W. Jr. and Thomas, J.T., "Effect of Twist and Camber on the Low-Speed Aerodynamic Characteristics of a Powered Close-Coupled Wing-Canard Configuration," NASA TM 78722, May 1978.

[3] Paulson, J.W. Jr., Thomas, J.L., and Winston, M.M., "Transition Aerodynamics for Close-Coupled Wing-Canard Configuration," AIAA Paper 79-0336, Jan. 1979.

[4] Whitten, P.D., "An Experimental Investigation of a Vectored-Engine-Over-Wing Powered-Lift Concept, Vol. II—High Angle of Attack and STOL Tests," U.S. Air Force AFFDL-TR-76-92, Vol. II, March 1978.

[5] Leavitt, L.D. and Yip, L.P., "Effects of Spanwise Nozzle Geometry and Location on the Longitudinal Aerodynamic Characteristics of a Vectored-Engine-Over-Wing Configuration at Subsonic Speeds," NASA TP 1215, May 1978.

[6] Whitten, P.D. and Howell, G.A., "Investigations of the VEO-Wing Concept in Air-To-Ground Role," U.S. Air Force AFFDL-TR-79-3031, March 1979.

[7] Stumpfl, S.C., "Vectored-Engine-Over-Wing Concept Development," *Proceedings V/STOL Aircraft Aerodynamics,* Vol. II, Naval Postgraduate School, Monterey, Calif., May 1979, p. 850.

[8] Whitten, P.D. and Howell, G.A., "Data Report for Low-Speed Test of the .108-Scale Vectored-Engine-Over-Wing Powered-Lift Research Model. Vol. 1—Force Data," General Dynamics/Ft. Worth Report FZA-501-Vol. 1, Sept. 1979.